Pyrrole $^{\beta}$C–B–N Fused Porphyrins: Molecular Structures and Opto-Electrochemical Studies

Rajendra Prasad Nandi,[a] Brijesh Chandra,[a] Subhajit Ghosh,[a] Siddhartha P. Sarma,[b] Silvano Geremia,[c] Neal Hickey,*[c] and Pakkirisamy Thilagar*[a]

Herein, we report the design, synthesis, structure, and electrochemical study of doubly $^{\beta}$C–B–N fused Ni(II) porphyrins (**1-trans**, **1-cis**, **2-trans**, and **2-cis**). These compounds have been synthesized from A_2B_2 type dipyridyl Ni(II) porphyrins (Ar=Ph for **1a**; Ar=C_6F_5 for **2a**) via Lewis base-directed electrophilic aromatic borylation reactions. The solution state structures of these compounds have been established using ^{1}H NMR, ^{11}B NMR, ^{1}H-^{1}H COSY, ^{1}H-^{13}C HSQC, and ^{19}F-^{13}C HSQC NMR techniques. Single crystal X-ray analysis have revealed that **1-trans**, **1-cis**, and **2-trans** adopt ruffled conformations, with alternate meso-carbons on the opposite sides of the mean porphyrin plane. The Soret bands in the absorption spectra of the B–N fused molecules are ~40 nm redshifted compared to unfused Ni(II) porphyrin precursors. The B–N fusion have diminished the redox potential of fused porphyrins. Although **1-trans** and **1-cis**, show four oxidation processes, **2-trans** and **2-cis** show only three oxidation processes. DFT studies have revealed that the tetrahedral geometry of the boron has induced a twist in the π-conjugation, which destabilizes the HOMO and stabilizes the LUMO in **1-trans**, **1-cis**, **2-trans**, and **2-cis**.

Introduction

Porphyrin, a tetrapyrrolic aromatic cyclic structure, widely known as the "Pigment of life", has continuously been modified to investigate its potential application in various fields. In particular, porphyrins with extended π-systems have recently attracted a lot of attention due to their redshifted absorption, which makes them potential candidates for various applications, e.g., infrared live-cell imaging, organic semiconductors, organic photovoltaic cells, etc.[1] π-Extension in porphyrins has generally been achieved in two main ways: 1) fusion with carbon-based aromatic rings[1e,f,2] and 2) fusion with heteroatoms.[3] Modification of porphyrins by insertion of fused aromatic rings on the periphery of porphyrin system has been intensively explored because of the advantages offered by the unique physical properties achieved due to narrowed HOMO–LUMO gap.[1e,f,2a] On the other hand, heteroatom fused porphyrins, especially fused with B, N, S, and P heteroatoms, have begun to receive attention in recent reports.[3–4] Intriguing optical and electrochemical properties are observed for these fused porphyrins.

Recently, B–N containing materials have attracted immense interest owing to their numerous applications in optoelectronics and biology.[5] One strategy to achieve BN-containing organic molecules is to substitute one or more C=C units with isoelectronic B–N units.[6] The B–N unit behaves as a zwitterionic double bond in the neutral state,[7] and maintains the primary olefin structural motif; but induces dramatically different optical and electronic properties due to the electronegative difference between boron and nitrogen.[8] Another strategy is to include a B–N coordinate bond comprising a tetracoordinate boron center. B–N fused π-conjugated systems with tetracoordinated boron have also been studied extensively, owing to their intriguing chemical and optical properties.[9] Recently, Jäkle and coworkers demonstrated the triplet oxygen sensitization of doubly B–N doped anthracenes.[10]

Boron-containing porphyrins show intriguing optical properties. Boron porphyrin hybrids with B(III) bonded to the pyrrole nitrogen, and placed inside the porphyrin core, are well established.[12] similarly with regard to boron units at the periphery of porphyrins, tri- and tetra- coordinate boron units are easily connected to the core/aryl (at meso positions) of porphyrins.[13] However, boron fused porphyrins have been very rarely realized. For example, Osuka *et al.* have demonstrated direct fusion of tricoordinate boron atoms between meso-carbons and aryl moieties (at the pyrrole β-carbon),[4] whereas Pawlicki and coworkers have reported a boron fused porphyrin system by entrapping boron in a predefined CNN coordination setting (Chart 1).[11] However, tetracoordinated boron fused porphyrins have not yet been reported. In the case of such tetracoordinated boron, although the empty p-orbital would not be available, the intrinsic tetrahedral geometry of the tetracoordinated boron may cause the porphyrin π-system to

[a] *Dr. R. P. Nandi, Dr. B. Chandra, S. Ghosh, Prof. P. Thilagar*
Department of Inorganic and Physical Chemistry
Indian Institute of Science
Bangalore – 560012, INDIA
E-mail: thilagar@iisc.ac.in

[b] *Prof. S. P. Sarma*
Molecular Biophysics Unit, Division of Biological Sciences
Indian Institute of Science
Bangalore – 560012, INDIA

[c] *Prof. S. Geremia, Dr. N. Hickey*
Department of Chemical and Pharmaceutical Sciences
University of Trieste
via L. Giorgieri 1 – 34127, Trieste, ITALY
E-mail: nhickey@units.it

twist and modify its optoelectronic properties.[14] Keeping these considerations in mind, we set out to investigate how the tetrahedral geometry of boron can affect the frontier molecular orbitals (FMOs) of B–N fused porphyrins.

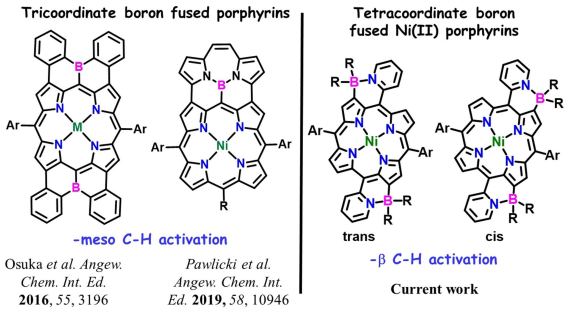

Chart 1. Structures of previously developed tricoordinate boron fused porphyrins[4, 11] and current strategy for designing tetracoordinate boron fused porphyrins.

One of the well-established methodologies to obtain *meso*-β fused porphyrins is the metal-catalyzed oxidative coupling of meso aryl with β-pyrrole C–H and vice versa.[2b] Unfortunately, this methodology is not suitable for making boron-fused porphyrins, as the organoboranes are not stable under such reaction conditions. In 2016, Osuka *et al.* have elegantly exploited Si–B exchange reactions to make tricoordinate boron-fused porphyrins (Chart 1).[4] On the other hand, B–N fused polyaryls can be conveniently synthesized via Lewis base-directed electrophilic aromatic borylation reactions.[10,15] In 2019, Pawlicki and coworkers have achieved boron-fused porphyrins through meso C–H activation by exploring this route.

In light of these considerations, we have chosen an A_2B_2 type porphyrin system with two meso carbons functionalized with 2-pyridyl moieties as precursors. We have envisioned that the Lewis base pyridyl nitrogen would direct the selective electrophilic borylation of pyrrole β-C–H of porphyrin and lead to the formation of B–N fused porphyrins. Accordingly, we have designed and synthesized Ni-Ar_2Py_2 porphyrins **1a** (Ar=C_6H_5) and **2a** (Ar=C_6F_5), and the electrophilic borylation of these porphyrins furnishes a mixture of geometric isomers **1-trans**, **1-cis**, **2-trans**, and **2-cis** (Scheme 1). We have successfully activated the β-pyrrolic C–H through borylation, which is more challenging than the activation of meso protons.[16] As anticipated, the tetracoordinated boron allows the porphyrin π-system to twist and modify the energy of FMOs. The intriguing molecular structure, optical properties and electrochemical properties of these B–N fused porphyrin isomers have been reported in this article.

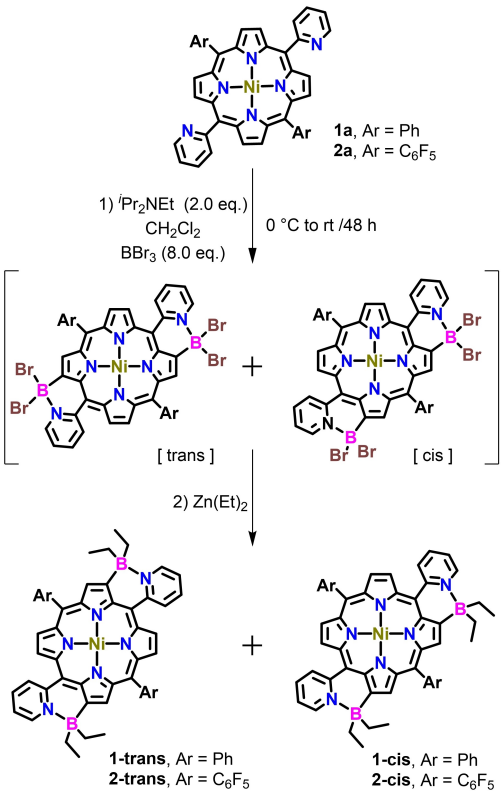

Scheme 1. Synthesis of doubly B–N fused porphyrins **1-trans**, **1-cis**, **2-trans**, and **2-cis**.

Results and Discussion

Synthesis and Characterization

The doubly B–N fused porphyrins **1-trans**, **1-cis**, **2-trans**, and **2-cis**, have been synthesized following the procedure depicted in Scheme 1. The precursor Ni-Ar_2Py_2 porphyrins **1a** and **2a** have been synthesized following the procedure reported in the literature (Scheme S1).[17] In short, condensation of aryldipyrromethane (**1c**; aryl=C_6H_5, and **2c**; aryl=C_6F_5) with pyridine-2-carboxaldehyde followed by oxidation with 2,3-dichloro-5,6-dicyano-1,4-benzoquinone (DDQ) produces **1b** and **2b**. The metal complexes **1a** and **2a** have been obtained by allowing **1b** and **2b** to react with anhydrous nickel salt ($NiCl_2$ for **1a**, $Ni(OAc)_2$ for **2a**). Finally, Lewis-base directed borylation of **1a**/**2a** with BBr_3 in the presence of $^iPr_2NEt$ followed by alkylation with $ZnEt_2$ results mixtures of **1-trans** and **1-cis**/**2-trans** and **2-cis** as dark green colored solids. The isomers have been successfully separated using basic alumina column chromatography.

The chemical structures of these compounds have been unequivocally established by high-resolution mass spectroscopy (HRMS), 1-D ^1H, ^{11}B NMR, ^1H–^1H COSY, ^1H–^{13}C HSQC, and ^{19}F–^{13}C HSQC NMR techniques (Figures S1–37). Furthermore, the solid-state molecular structures of **1-trans**, **1-cis**, and **2-trans** have been confirmed by single-crystal x-ray diffraction studies (Figure S38). In the ^1H NMR spectra, the protons of the boron fused pyrrole rings are upfield shifted compared to the protons of the pyrrole moiety not connected to boron (Figure S12, 29). This result signifies that the tetracoordinated boron fusion causes modification of the electron density distribution of the porphyrin macrocycle. The cis and trans isomers for both phenyl and pentafluorophenyl derivatives show distinct peaks in ^1H NMR spectra (Figure S12, 29). ^{13}C resonances for all the borylated compounds are studied by the ^1H-^{13}C HSQC technique (Fig-

ure S7, 11, 21, and 27). However, peaks for $-CH_2-$ groups are not observed as they are connected to quadruple boron nuclei. ^{11}B NMR for all the compounds show broad signals at ~2–4 ppm (1.5, 2.2, 4.1, and 2.0 ppm for **1-trans, 1-cis**, **2-trans** and **2-cis**, respectively, Figures S5, 9, 18, and 24) which are in line with the reported tetracoordinate boron containing B–N molecules.[10] In ^{19}F NMR spectra, **2-trans** (Figure S19) shows three similar peaks to the precursors **2 b** (Figure S14) and **2 a** (Figure S16). However, **2-cis** (Figure S25) shows four peaks. The most downfield shifted peaks in the range of −135 to −140 ppm can be assigned to the ortho fluorine atoms ('a') as they are the most deshielded by the porphyrin ring current, and the most upfield shifted peaks in the range of −160 to −165 ppm could be due to the meta- fluorine atoms ('b'). The triplets in the range of −150 to −155 ppm are attributable to the para fluorine atoms ('c'/'d').[18] Possibly, the chemical shift of para fluorine atoms are governed by the electronic effect of porphyrin ring and which is similar for both fluorine atoms in **2-trans** (one triplet) and different in **2-cis** (two triplets). $^{19}F-^{13}C$ HSQC spectrum dictates the signals corresponding to the carbon atoms attached to the fluorine atoms (Figures S22, S28).

Single crystals suitable for X-ray diffraction have been obtained by slow evaporation of solutions of **1-trans**, **1-cis**, and **2-trans** using CH_2Cl_2/DMSO, CH_2Cl_2 and ethylacetate/methanol solvents, respectively. The molecular structures of these compounds have been determined using X-ray radiation from synchrotron (**1-trans**, **2-trans**) or conventional sources (**1-cis**) (Figures 1, S38).[19] Compound **1-trans** are found to crystallize in the triclinic *P-1* space group, while compounds **1-cis** and **2-trans** crystallize in the same monoclinic space group and are refined as $P2_1/n$ *and* $P2_1/c$, respectively. Two crystallographically distinct molecules are present in the asymmetric units of **1-trans**, and **2-trans**, while **1-cis** contains just one. Crystal structures of nickel(II)porphyrins with direct meso-fused tricoordinate boron have been previously reported.[4] These compounds adopt a saddle-shape conformation; however, unlike these compounds, the doubly tetracoordinated boron fused **1-trans**, **1-cis**, and **2-trans** adopt ruffled structures. The meso carbons in **1-trans**, **1-cis**, and **2-trans** are alternately displaced above and below the mean porphyrin plane, typical of the ruffled porphyrin structure (Figures S39–41).[20] The displacement of the meso carbons from the mean porphyrin plane respectively, whereas for **1-cis** the displacements are slightly higher in the range 0.734–0.865 Å (Table S2). The dihedral angles between the pyrrole rings and the mean porphyrin plane in **1-trans** (20.5–22.6°), **2-trans** (19.6–22.5°) and **1-cis** (24.7–25.7°) are in line with values reported for structure with ruffled porphyrin core (Figures S45–47. Table S4).[14a] The meso- phenyl rings in **1-trans/1-cis** and the $-C_6F_5$ moiety in **2-trans** are placed almost perpendicular to the mean porphyrin plane (Figures S42–44. Table S3). In contrast, the fused pyridyl rings adopt moderate coplanarity with the porphyrin plane (33.3–43.7°), indicating the possible extended π-conjugation between these two rings. Geometric details of the ruffled conformations of the three structures are given in Tables S2–S4.

The sp^3 hybridized boron centres in all these compounds adopt tetrahedral geometry (Table S5). The B–C_β bond distances (**1-trans**: 1.588(2)–1.593(2) Å; **1-cis**: 1.563(1)–1.598(1) Å; **2-trans**: 1.578(1)–1.585(1) Å) are significantly shorter than the B–C(Et) (**1-trans**: 1.616(2)–1.634(2) Å; **1-cis**: 1.618–1.636 Å; **2-trans**: 1.606(2)–1.654(1) Å). This indicates the possible delocalization of porphyrin π electrons towards the boron centre. The B–N bond distances of 1.631(2)–1.648(2) Å in **1-trans**, 1.628(2)–1.653(1) Å in **2-trans**, and 1.641(1)–1.654(1) Å in **1-cis** are in line with other tetracoordinate B–N based molecules.[10]

Optical Properties

UV-vis absorption spectra of all the synthesized porphyrins have been recorded in dichloromethane at ambient conditions (Figures 2, S48–49). The electronic absorption spectrum of these compounds exhibits absorption in two distinct regions similar to previously reported typical porphyrin systems. Free-base porphyrins show an intense Soret band (**1 b**: 417 nm and **2 b**: 415 nm) and four Q-bands, while the Ni-Porphyrins show only two Q-bands typical of metalloporphyrins. However, the doubly B–N fused Ni-porphyrins **1-trans, 1-cis**, **2-trans**, and **2-cis** show stronger redshifted Q-bands with respect to those observed for Ni-Porphyrins **1 a** and **2 a**. Compounds **1-trans, 1-cis**, **2-trans**, and **2-cis**, are also characterized by intense and redshifted Soret bands. These redshifted UV-Vis absorption in **1-trans**, **1-cis**, **2-trans**, and **2-cis** are due to the extended conjugation of porphyrin macrocycle through pyridine-boron. These observations are further supported by theoretical calculations (vide infra). Similar red shifted absorption and emission are observed for the boron-fused porphyrins and other π-extended porphyrins reported in the literature.[1a–e,4,11]

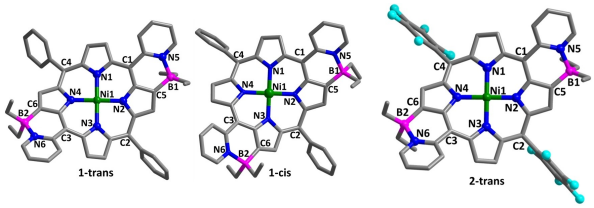

Figure 1. Molecular structures of **1-trans, 1-cis**, and **2-trans**. Atom colour code: C-grey, N-blue, Ni-green, B-purple, F-cyan.

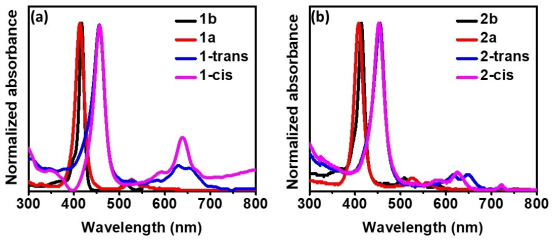

Figure 2. Normalized UV-vis absorption spectra of all the compounds in dichloromethane (conc. = 1 μM).

Theoretical Calculation

To understand the influence of B–N fusion and conformational features of the porphyrin macrocycles, the S_0 state geometries of each synthesized porphyrin have been optimized using b3lyp functional and 6311 + g(d,p) (and LanL2DZ for Ni) basis set in the gas phase (Figures 3, S50). The geometric parameters of the optimized structures of **1-trans**, **1-cis**, and **2-trans** match well with crystallographic data. The frontier molecular orbitals (FMOs) in **1 b**, **1 a**, **2 b**, and **2 a** are localized on the porphyrin macrocycle with negligible contribution from meso substituents. In all four B–N fused compounds, HOMO and LUMO + 1 are mainly localized on the Ni-porphyrin macrocycle with minimal contribution from the B–N fused rings. However, HOMO-1 and LUMO are delocalized over the Ni-porphyrin macrocycle and pyridyl-BEt_2-Cβ rings with negligible contribution from meso aryl moieties (Figures 3, S50). The HOMOs of **1-trans**, **1-cis**, **2-trans**, and **2-cis** are all destabilized, whereas the LUMO of these compounds is highly stabilized with respect to those of **1 a** and **2 a**. This leads to an overall decrease in the HOMO-LUMO band gap in all four compared to **1 a** and **2 a**. These initial studies reveal that ring fusion through boron insertion can effectively alter the FMOs of the B–N fused porphyrins and can significantly reduce the HOMO-LUMO gap. The anisotropy of the induced current density (AICD) calculation has been performed on all the molecules. The clockwise diamagnetic current flow in the calculated ACID plots (Figure S53) indicates the aromatic nature of all the molecules. Although the AICD plots do not indicate the extended conjugation prominently, forced coplanarity of pyridine with the porphyrin rings through B–N fusion in **1-trans**, **1-cis**, **2-trans**, and **2-cis** is evident from these plots, which increases the possibility of extended conjugation. TD-DFT calculations (Table S7) have suggested that transition probabilities (*f*) corresponding to the lower singlet excited states are quite low (**1 b**: S1–S2; **1 a**: S1–S5; **1-trans**: S1–S5; **1-cis**: S1–S5), which corroborates the low intensity of the Q bands. On the other hand, the transition probabilities (*f*) for some higher singlet excited states are quite high (**1 b**:S3–S4; **1 a**: S10–S12; **1-trans**: S12–S13; **1-cis**: S11–S13), which are accountable for the strong Soret bands for these molecules. Similar observations have been noted for **2 b**, **2 a**, **2-trans**, and **2-cis** as well.

Electrochemical Properties

These porphyrins have been characterized by cyclic voltammetry (CV) and differential pulse voltammetry (DPV) in dichloromethane containing supporting electrolyte tetrabutyl ammonium hexafluorophosphate (Figures 4, S54). Compounds **1 b** and **1 a** show two one-electron oxidation processes (for **1 b**, (E_{ox1}: 0.43 and E_{ox2}: 0.74 V, for **1 a** E_{ox1}: 0.48 and E_{ox2}: 0.78 V) and two one-electron reduction processes (for **1 b**, E_{red1}: −1.55 and E_{red2}: −1.91 V, for **1 a** E_{red1}: −1.57 and E_{red2}: −1.99 V) centered on porphyrin, similar to the other reported porphyrins and Ni-porphyrins.[21]

The B–N fused compounds **1-trans**, **1-cis**, **2-trans**, and **2-cis** show two reduction peaks similar to **1 a** and **2 a** (Figures 4, S54,

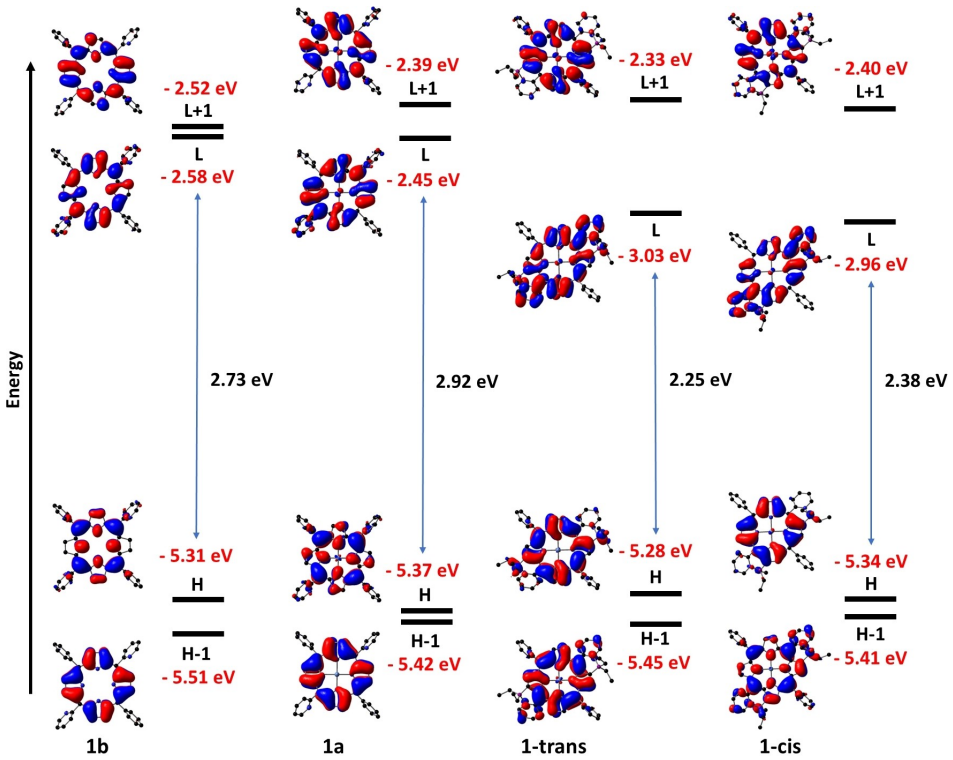

Figure 3. Frontier molecular orbitals (H: HOMO, L: LUMO) of porphyrins **1 b, 1 a, 1-trans** and **1-cis**. DFT calculations have been performed in Gaussian 16 using b3lyp functional and 6-311 + g(d,p) basis set for C, H, N, B and Lanl2dz basis set for Ni atoms.

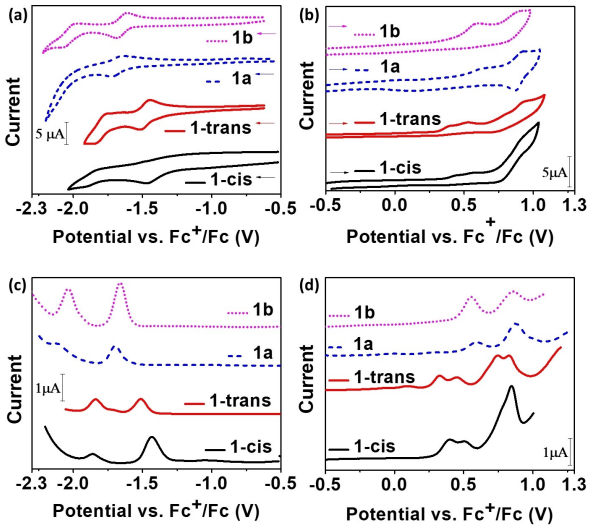

Figure 4. Cyclic voltammetry (a, b) and differential pulse voltammetry (c, d) of **1 b**, **1 a**, **1-trans** and **1-cis** (reduction: a and c, oxidation: b and d).

and Table S8). However, the half-wave potential of the borylated compounds indicates that these compounds are easy to reduce compared to precursors devoid of B–N fused rings, which can be attributed to the more stabilized LUMO in B–N fused compounds compared to the non-borylated compounds. Compounds **2-trans** and **2-cis** can be more easily reduced than **1-trans** and **1-cis**. This result is consistent with the difference in the electron-withdrawing properties of meso-aryl moieties in these compounds. The easiest reduction is expected for **2-trans** and **2-cis** with strongly electron-withdrawing $-C_6F_5$ substituents, while it should be more difficult for **1-trans** and **1-cis** with simple $-C_6H_5$ substituents.

Surprisingly, **1-trans** and **1-cis**, show four irreversible oxidation peaks, whereas **2-trans** and **2-cis** show three irreversible oxidation processes (Figures 4, S54, S55, S56, Table S8). The oxidation potentials of these compounds indicate that these compounds are easier to oxidize than the Ni-porphyrin precursors. Furthermore, **2-trans** and **2-cis**, with strongly electron-withdrawing meso-C_6F_5 substituents, are more difficult to oxidize compared to **1-trans** and **1-cis** with simple meso-C_6H_5 substituents. However, the unexpected phenomenon is that **2-trans** and **2-cis** show third oxidation processes, and **1-trans** and **1-cis** show third and fourth oxidation processes. However, these additional oxidation curves do not originate from Ni(II)→Ni(III) oxidation as Ni center oxidation can be achieved only at very low temperature and/or at high potential (> 1.5 V vs SCE).[21] Similar splitting of the oxidation peaks have been exhibited by porphyrin dimers due to the coulombic interaction between the positive charge in one porphyrin ring of the monocation radical produced during the first oxidation and the electron to be extracted from another porphyrin ring during the second oxidation, as reported by Osuka *et al.*, and Chmielewski *et al.*[22] However, these oxidation peaks are reversible in nature, and are not observed for any other porphyrin monomer or other β-fused porphyrins. Further, although tri and tetra anions have been reported for porphyrins with strong electron-withdrawing substituents and doubly fused chlorine,[23] this does not seem to be the case here.

These oxidation potentials are strongly dependent on the nature of the meso-aryl group attached to the core. The easiest oxidation is expected for **1-trans** and **1-cis** with simple $-C_6H_5$ substituents, and the hardest for the **2-trans** and **2-cis**, with strongly electron-withdrawing $-C_6F_5$ substituents. Furthermore, compounds **2-trans** and **2-cis**, with electron-withdrawing $-C_6F_5$ substituents are expected to have the fourth oxidation at much higher potentials and which is probably beyond the available electrochemical potential window of current experimental set up; consequently, the fourth oxidation have not been observed. Although the oxidation peaks are irreversible in nature when recorded separately in different potential window, but their unchanged potential (e.g., 2nd oxidation followed by 1st oxidation versus 2nd oxidation separately) indicates that these oxidations are originating from different part of the molecules (Figures S55, S56). The different distribution of molecular orbitals can affect the redox behaviors[22a]. Preliminary DFT studies suggest that the Et_2B-C_5NH_4 moiety contributes significantly to the HOMO-2 and HOMO-3 orbitals (Figures S51–53). Based on these results, the first two oxidations are proposed to be located at the porphyrin macrocycle and the additional oxidations at the B–N fused rings, each oxidation occurring at a different potential, consistent with the characteristics of two interacting oxidation centres.

Conclusions

We have successfully designed and synthesized doubly B–N fused Ni(II) porphyrin isomers **1-trans**, **1-cis**, **2-trans**, and **2-cis**. The chemical structure of these compounds have been established using ^{1}H NMR, ^{11}B NMR, ^{1}H–^{1}H COSY, ^{19}F–^{13}C HSQC, and ^{1}H–^{13}C HSQC NMR techniques. Both single crystal structure determination and DFT calculations have revealed that the porphyrin core in these compounds adopts ruffled shape conformation. The tetracoordinated boron fusion strongly stabilizes the LUMO, with a consequent redshift in UV-vis absorption compared to compounds without B–N fusion. Electrochemical studies revealed that B–N fused Ni(II) porphyrins are easier to oxidize and easier to reduce than Ni(II) porphyrins. Our designed strategy could further pave the way for new near IR emitting materials by employing appropriate metal centers and/or suitable substituents on the boron center.

Experimental Section

Synthesis of Nickel Porphyrin 1 a: Porphyrin **1 b** (200 mg, 0.32 mmol) and anhydrous $NiCl_2$ (2.10 g, 16.21 mmol) was dissolved in 30 ml of anhydrous dimethyl formamide under nitrogen atmosphere and refluxed for 24 hrs. Upon cooling to room temperatures, nickel porphyrin **1 c** was precipitated out, which was filtered and washed with methanol to obtain pure product. Yield = 130 mg (60 %). **^{1}H NMR** (400 MHz, $CDCl_3$) δ: 9.07 (d, 2H, J = 5.0 Hz), 8.76 (s, 8H), 8.03–8.00 (m, 6H), 7.95 (d, 2H, J = 7.6 Hz), 7.72–7.66 (m, 6H), 7.64–7.63 (m, 2H). **^{13}C NMR** (125 MHz, $CDCl_3$) δ: poor signal due to

poor solubility and presence of significant numbers of quaternary carbons. However, $^{1}H–^{13}C$ HSQC spectra depicted in figure S3 gives the ^{13}C signals corresponding to carbons attached to hydrogens. **HRMS** (ESI) m/z: $[M+H]^+$ calcd. for $C_{42}H_{26}N_6Ni$ 673.1651; found 673.1654.

Synthesis of B–N porphyrin 1-trans and 1-cis: Nickel porphyrin **1 a** (120 mg, 0.18 mmol) was dissolved in 40 mL of anhydrous dichloromethane under nitrogen atmosphere followed by the addition of N,N-diisopropylethylamine (62 μL, 0.36 mmol). The solution was cooled to 0 °C and BBr_3 (135 μL, 1.43 mol) was added with stirring. The reaction mixture was then warmed to 25 °C and stirred for 72 hrs. at the same temperature. Then the mixture was cooled to 0 °C and diethyl zinc (1.0 M in hexane) (5.35 ml, 5.35 mmol) was added followed by warming to 25 °C. The reaction mixture was stirred for another 48 hrs and was quenched by water upon completion. The product was extracted with dichloromethane and the organic fraction was separated washed with water followed by evaporation to give the crude product. Purification was performed using basic alumina column and 5% ethyl acetate/hexane as eluent to obtain both the isomers **1-trans** (13.0 mg, yield = 9%) and **1-cis** (8.0 mg, yield = 5%) in pure form. Characterization data for **1-trans**: **^{1}H NMR** (400 MHz, $CDCl_3$) δ: 9.09 (d, 2H, J = 4.9 Hz), 9.04 (d, 2H, J = 5.8 Hz), 8.68 (d, 2H, *J* = 4.9 Hz), 8.46 (s, 2H), 8.13–8.05 (m, 6H), 7.70 (brs, 8H), 7.55–7.51 (m, 2H), 1.05–1.02 (m, 8H), 0.62 (brs, 12H). **^{13}C NMR** (125 MHz, $CDCl_3$) δ: weak signal due to poor solubility and presence of significant numbers of quaternary carbons. However, $^{1}H–^{13}C$ HSQC spectra depicted in figure S7 gives the ^{13}C signals corresponding to the carbons attached to hydrogens. **^{11}B NMR** (128 MHz, $CDCl_3$) δ: 1.49 ppm. **HRMS** (ESI) m/z: $[M+H]^+$ calcd. for $C_{50}H_{45}B_2N_6Ni$ 809.3245; found 809.3246. Characterization data for **1-cis**: **^{1}H NMR** (500 MHz, $CDCl_3$) δ: 9.04 (d, 2H, J = 4.8 Hz), 9.01 (d, 2H, J = 5.8 Hz), 8.62 (d, 2H, *J* = 4.8 Hz), 8.43 (s, 2H), 8.12–8.04 (m, 6H), 7.70–7.69 (m, 8H), 7.52–7.49 (m, 2H), 1.02–0.98 (m, 8H), 0.62 (brs, 12H). **^{13}C NMR** (125 MHz, $CDCl_3$) δ: weak signal due to poor solubility and presence of significant numbers of quaternary carbons. However, $^{1}H–^{13}C$ HSQC spectra depicted in figure S11 gives the ^{13}C signals corresponding to the carbons attached to hydrogens. **^{11}B NMR** (128 MHz, $CDCl_3$) δ: 2.24 ppm **HRMS** (ESI) m/z: $[M+H]^+$ calcd. for $C_{50}H_{45}B_2N_6Ni$ 809.3245; found 809.3221.

Synthesis of nickel porphyrin 2 a: Porphyrin **2 b** (250 mg, 0.31 mmol) and anhydrous $NiCl_2$ (488 mg, 3.77 mmol) was dissolved in 120 ml of anhydrous dimethyl sulfoxide under nitrogen atmosphere and heated at 160 °C for 3 hrs. After reaction completion the solvent was evaporated under vacuum and the residue solid was extracted with ethyl acetate followed by washing with water. The crude product was purified over basic alumna column using 5% ethyl acetate/chloroform as eluent to give pure Nickel porphyrin **2 a**. Yield = 160 mg (60%). Characterization data: **^{1}H NMR** (400 MHz, $CDCl_3$) δ: 9.09 (d, 2H, J = 4.2 Hz), 8.86 (d, 4H, J = 5.0 Hz), 8.70 (d, 4H, J = 5.0 Hz) 8.08–8.04 (m, 2H), 7.98 (d, 2H, J = 7.7 Hz). **^{13}C NMR** (125 MHz, $CDCl_3$) δ: 159.2, 149.1, 147.7, 145.2, 143.4, 142.5, 135.4, 133.7, 131.3, 129.8, 123.1, 118.9, 102.3. **^{19}F NMR** (470 MHz, $CDCl_3$) δ: −136.82 (dd, 6.4 Hz, 23.6 Hz), −152.33 (t, 20.7 Hz), 161.79 (dt, 4.1 Hz, 22.0 Hz) **HRMS** (ESI) m/z: $[M+H]^+$ calcd. for $C_{42}H_{17}F_{10}N_6Ni$ 853.0708; found 853.0710.

Synthesis of B-N porphyrin 2-trans and 2-cis: B–N porphyrin **2-trans** and **2-cis** were synthesized in analogy to the procedure for **1-trans** and **1-cis**. Reagents used, and characterization data are as follows: Nickel porphyrin **2 a** (100 mg, 0.12 mmol), N,N-diisopropylethylamine (41 μL, 0.23 mmol), BBr_3 (89 μL, 0.94 mol) diethyl zinc (1.0 M in hexane) (3.52 ml, 3.52 mmol). Product obtained: **2-trans** (14.0 mg, yield = 12%) and **2-cis** (8.0 mg, yield = 7%). Characterization data for **2-trans**: **^{1}H NMR** (500 MHz, $CDCl_3$) δ: 9.18 (d, 2H, J = 4.8 Hz), 9.09 (d, 2H, J = 5.8 Hz), 8.61 (d, 2H, *J* = 4.7 Hz), 8.35 (s, 2H), 8.14–8.12 (m, 4H), 7.61–7.59 (m, 2H), 1.06 (brs, 8H), 0.63 (brs, 12H). **^{13}C NMR** (125 MHz, $CDCl_3$) δ: weak signal due to poor solubility, presence of significant numbers of quaternary carbons, and splitting due to the $-C_6F_5$ group. However, $^{1}H–^{13}C$ HSQC spectra depicted in figure S21 gives the ^{13}C signals corresponding to the carbons attached to hydrogens, and $^{19}F–^{13}C$ HSQC spectra depicted in figure S22 gives the ^{13}C signals corresponding to the carbons attached to fluorines. **^{11}B NMR** (128 MHz, $CDCl_3$) δ: 4.14 ppm. **^{19}F NMR** (470 MHz, $CDCl_3$) δ: −137.06 (brs), −152.81 (t, 20.9 Hz), 161.77 (brs). **HRMS** (ESI) m/z: $[M+H]^+$ calcd. for $C_{50}H_{35}B_2F_{10}N_6Ni$ 989.2303; found 989.2300. Characterization data for **2-cis**: **^{1}H NMR** (500 MHz, $CDCl_3$) δ: 9.13 (d, 2H, J = 4.5 Hz), 9.07 (d, 2H, J = 5.2 Hz), 8.56 (d, 2H, *J* = 4.8 Hz), 8.31 (s, 2H), 8.13–8.12 (m, 4H), 7.62–7.59 (m, 2H), 1.04 (brs, 8H), 0.63 (brs, 12H). **^{13}C NMR** (125 MHz, $CDCl_3$) δ: spectra could not be recorded due to poor solubility, presence of significant numbers of quaternary carbons, and splitting due to the $-C_6F_5$ group. However, $^{1}H–^{13}C$ HSQC spectra depicted in figure S27 gives the ^{13}C signals corresponding to the carbons attached to hydrogens, and $^{19}F–^{13}C$ HSQC spectra depicted in figure S28 gives the ^{13}C signals corresponding to the carbons attached to fluorines. **^{11}B NMR** (128 MHz, $CDCl_3$) δ: 1.98 ppm **^{19}F NMR** (470 MHz, $CDCl_3$) δ: −137.00 (d, 22.8 Hz), −152.37 (t, 20.8 Hz), −153.29 (t, 20.7 Hz), 161.91 (brs). **HRMS** (ESI) m/z: $[M+H]^+$ calcd. for $C_{50}H_{35}B_2F_{10}N_6Ni$ 989.2303; found 989.2304.

Acknowledgements

RPN thanks IISc Bangalore, India, for a research fellowship, BC thanks UGC, New Delhi, India, for a Dr. D. S. Kothari Post-Doctoral Fellowship, SG thanks Govt. of India for PMRF and PT thanks SERB New Delhi, India, for research funding and IISc for Infrastructure. SG and NH thank the Elettra Synchrotron (Trieste, Italy) and the staff of the XRD1 beamline for their technical assistance.

Conflict of Interests

The authors declare no conflict of interest.

Data Availability Statement

The data that support the findings of this study are available in the supplementary material of this article.

Keywords: Ni(II) Porphyrin · B–N fusion · Boron · $^{\beta}$C–H activation · Electrochemical Potential

[1] a) Y. Kurumisawa, T. Higashino, S. Nimura, Y. Tsuji, H. Iiyama, H. Imahori, *J. Am. Chem. Soc.* **2019**, *141*, 9910–9919; b) T. Ishizuka, Y. Saegusa, Y. Shiota, K. Ohtake, K. Yoshizawa, T. Kojima, *Chem. Commun.* **2013**, *49*, 5939–5941; c) J. Li, N. Merino-Diez, E. Carbonell-Sanroma, M. Vilas-Varela, D. G. de Oteyza, D. Pena, M. Corso, J. I. Pascual, *Sci. Adv.* **2018**, *4*, eaaq0582; d) A. M. Huerta-Flores, G. Bengasi, K. Baba, N. D. Boscher, *ACS Appl. Energ. Mater.* **2020**, *3*, 9848–9855; e) H. Mori, T. Tanaka, A. Osuka, *J. Mater. Chem. C* **2013**, *1*; f) S. A. Balahoju, Y. K. Maurya, P. J. Chmielewski, T. Lis, M. Kondratowicz, J. Cybinska, M. Stepien, *Angew. Chem. Int. Ed.* **2022**, *61*, e202200781.

[2] a) D. Mysliwiec, B. Donnio, P. J. Chmielewski, B. Heinrich, M. Stepien, *J. Am. Chem. Soc.* **2012**, *134*, 4822–4833; b) N. K. Davis, A. L. Thompson, H. L. Anderson, *J. Am. Chem. Soc.* **2011**, *133*, 30–31.

[3] a) K. Fujimoto, A. Osuka, *Chem. Sci.* **2017**, *8*, 8231–8239; b) M. Berthelot, G. Hoffmann, A. Bousfiha, J. Echaubard, J. Roger, H. Cattey, A. Romieu, D. Lucas, P. Fleurat-Lessard, C. H. Devillers, *Chem. Commun.* **2018**, *54*, 5414–5417; c) C. H. Chen, F. P. Gabbaï, *Chem. Sci.* **2018**, *9(29)*, 6210–6218; d) C. H. Chen, F. P. Gabbaï, *Angew. Chem. Int. Ed.* **2018**, *130(2)*, 530–534; e) M. Sakai, M. Mori, M. Hirai, N. Ando, S. Yamaguchi, *Chem. Eur. J.* **2022**, *28(38)*, e202200728.

[4] K. Fujimoto, J. Oh, H. Yorimitsu, D. Kim, A. Osuka, *Angew. Chem. Int. Ed.* **2016**, *55*, 3196–3199.

[5] a) Y. Chen, W. Chen, Y. Qiao, X. Lu, G. Zhou, *Angew. Chem. Int. Ed.* **2020**, *59*, 7122–7130; b) T. Hatakeyama, S. Hashimoto, S. Seki, M. Nakamura, *J. Am. Chem. Soc.* **2011**, *133*, 18614–18617; c) C. R. McConnell, S. Y. Liu, *Chem. Soc. Rev.* **2019**, *48*, 3436–3453; d) Y. Min, C. Dou, D. Liu, H. Dong, J. Liu, *J. Am. Chem. Soc.* **2019**, *141*, 17015–17021; e) M. Kawashiro, T. Mori, M. Ito, N. Ando, S. Yamaguchi, *Angew. Chem. Int. Ed.* **2023**, *135(26)*, e202303725; f) Y. Sugihara, N. Inai, M. Taki, T. Baumgartner, R. Kawakami, T. Saitou, T. Imamura, T. Yanai, S. Yamaguchi, *Chem. Sci.* **2021**, *12(18)*, 6333–6341; g) T. Hatakeyama, S. Hashimoto, T. Oba, M. Nakamura, *J. Am. Chem. Soc.* **2012**, *134*, 19600–19603; h) Y. Si, G. Yang, *J. Mater. Chem. C.* **2013**, *1*, 2354–2361; i) B. Adelizzi, P. Chidchob, N. Tanaka, B. A. Lamers, S. C. Meskers, S. Ogi, A. R. Palmans, S. Yamaguchi, E. W. Meijer, *J. Am. Chem. Soc.* **2020**, *142(39)*, 16681–16689; j) Z. Sun, C. Yi, Q. Liang, C. Bingi, W. Zhu, P. Qiang, D. Wu, F. Zhang, *Org. Lett.* **2020**, *22*, 209–213; k) M. Yang, I. S. Park, T. Yasuda, *J. Am. Chem. Soc.* **2020**, *142*, 19468–19472; l) J. K. Li, X. Y. Chen, Y. L. Guo, X. C. Wang, A. C. H. Sue, X. Y. Cao, X. Y. Wang, *J. Am. Chem. Soc.* **2021**, *143*, 17958–17963; m) S. Griesbeck, E. Michail, C. Wang, H. Ogasawara, S. Lorenzen, L. Gerstner, T. Zang, J. Nitsch, Y. Sato, R. Bertermann, M. Taki, *Chem. Sci.* **2019**, *10(20)*, 5405–5422.

[6] a) P. Ganesan, D.-G. Chen, W.-C. Chen, P. Gnanasekaran, J.-A. Lin, C.-Y. Huang, M.-C. Chen, C.-S. Lee, P.-T. Chou, Y. Chi, *J. Mater. Chem. C* **2020**, *8*, 4780–4788; b) Y. J. Lien, T. C. Lin, C. C. Yang, Y. C. Chiang, C. H. Chang, S. H. Liu, Y. T. Chen, G. H. Lee, P. T. Chou, C. W. Lu, Y. Chi, *ACS Appl. Mater. Interfaces* **2017**, *9*, 27090–27101; c) Q. Sun, L.-S. Cui, Y.-M. Xie, J.-J. Liang, Z.-q. Jiang, L.-s. Liao, M.-K. Fung, *Org. Electron.* **2017**, *48*, 112–117; d) H. Helten, *Chem. Eur. J.* **2016**, *22*, 12972–12982; e) D. H. Knack, J. L. Marshall, G. P. Harlow, A. Dudzik, M. Szaleniec, S. Y. Liu, J. Heider, *Angew. Chem. Int. Ed.* **2013**, *52*, 2599–2601; f) X. Y. Wang, H. R. Lin, T. Lei, D. C. Yang, F. D. Zhuang, J. Y. Wang, S. C. Yuan, J. Pei, *Angew. Chem. Int. Ed.* **2013**, *52*, 3117–3120; g) C. W. Hamilton, R. T. Baker, A. Staubitz, I. Manners, *Chem. Soc. Rev.* **2009**, *38*, 279–293; h) K. K. Neena, P. Sudhakar, P. Thilagar, *Angew. Chem. Int. Ed.* **2018**, *57*, 16806–16810; i) K. K. Neena, P. Sudhakar, K. Dipak, P. Thilagar, *Chem. Commun.* **2017**, *53*, 3641–3644; j) N. K. Kalluvettukuzhy, P. Thilagar, *Organometallics* **2017**, *36*, 2692–2701; k) K. K. Neena, P. Thilagar, *J. Mater. Chem. C* **2016**, *4*, 11465–11473; l) E. Fresta, J. Dosso, J. Cabanillas-González, D. Bonifazi, R. D. Costa, *Adv. Funct. Mater.* **2020**, *30*.

[7] J. Liu, X. Feng, *Angew. Chem. Int. Ed.* **2020**, *59*, 23386–23401.

[8] a) G. Bélanger-Chabot, H. Braunschweig, D. K. Roy, *Eur. J. Inorg. Chem.* **2017**, *2017*, 4353–4368; b) K. Niedenzu, *Angew. Chem. Int. Ed.* **1964**, *3*, 86–92; c) M. J. D. Bosdet, W. E. Piers, *Can. J. Chem.* **2009**, *87*, 8–29; d) Z. Liu, T. B. Marder, *Angew. Chem. Int. Ed.* **2008**, *47*, 242–244.

[9] a) V. Mukundam, S. Sa, A. Kumari, R. Das, K. Venkatasubbaiah, *J. Mater. Chem. C* **2019**, *7*, 12725–12737; b) Y. Li, H. Meng, D. Yan, Y. Li, B. Pang, K. Zhang, G. Luo, J. Huang, C. Zhan, *Tetrahedron* **2018**, *74*, 4308–4314; c) M. Yusuf, K. Liu, F. Guo, R. A. Lalancette, F. Jakle, *Dalton Trans.* **2016**, *45*, 4580–4587; d) C. Zhu, Z. H. Guo, A. U. Mu, Y. Liu, S. E. Wheeler, L. Fang, *J. Org. Chem.* **2016**, *81*, 4347–4352; e) N. Bäumer, S. Ogi, L. Borsdorf, S. Yamaguchi, G. Fernandez, *Chem. Commun.* **2023**, *59*, 8937–8940; f) J. Full, S. P. Panchal, J. Götz, A. M. Krause, A. Nowak-Król, *Angew. Chem. Int. Ed.* **2021**, *60*, 4350–4357; g) C. Shen, M. Srebro-Hooper, M. Jean, N. Vanthuyne, L. Toupet, J. A. G. Williams, A. R. Torres, A. J. Riives, G. Muller, J. Autschbach, J. Crassous, *Chem. Eur. J.* **2017**, *23*, 407–418; h) F. Full, Q. Wölflick, K. Radacki, H. Braunschweig, A. Nowak-Król, *Chem. Eur. J.* **2022**, *28*, e202202280; i) F. Full, M. J. Wildervanck, D. Volland, A. Nowak-Król, *Synlett.* **2022**, *33*, 477–482.

[10] a) K. Liu, R. A. Lalancette, F. Jakle, *J. Am. Chem. Soc.* **2017**, *139*, 18170–18173; b) K. Liu, R. A. Lalancette, F. Jakle, *J. Am. Chem. Soc.* **2019**, *141*, 7453–7462.

[11] W. Stawski, K. Hurej, J. Skonieczny, M. Pawlicki, *Angew. Chem. Int. Ed.* **2019**, *58*, 10946–10950.

[12] a) A. Sinha, T. Chatterjee, M. Ravikanth, *Coord. Chem. Rev.* **2022**, *465*; b) P. J. Brothers, *Chem. Commun.* **2008**, 2090–2102 ; c) A. Mlodzianowska, L. Latos-Grazynski, L. Szterenberg, M. Stepien, *Inorg. Chem.* **2007**, *46*, 6950–6957.

[13] a) Y. Kubo, M. Yamamoto, M. Ikeda, M. Takeuchi, S. Shinkai, S. Yamaguchi, K. Tamao, *Angew. Chem. Int. Ed.* **2003**, *42*, 2036–2040; b) P. C. Swamy, S. Mukherjee, P. Thilagar, *Anal. Chem.* **2014**, *86*, 3616–3624; c) K. Fujimoto, H. Yorimitsu, A. Osuka, *Chem. Eur. J.* **2015**, *21*, 11311–11314; d) C. A. P, P. Thilagar, *Dalton Trans.* **2016**, *45*, 4688–4696.

[14] a) W. Jentzen, M. C. Simpson, J. D. Hobbs, X. Song, T. Ema, N. Y. Nelson, C. J. Medforth, K. M. Smith, M. Veyrat, M. Mazzanti, R. Ramasseul, J. C. Marchon, T. Takeuchi, W. A. Goddard 3rd, J. A. Shelnutt, *J. Am. Chem. Soc.* **1995**, *117*, 11085–11097; b) T. Ishizuka, N. Grover, C. J. Kingsbury, H. Kotani, M. O. Senge, T. Kojima, *Chem. Soc. Rev.* **2022**, *51*, 7560–7630.

[15] N. Ishida, T. Moriya, T. Goya, M. Murakami, *J. Org. Chem.* **2010**, *75*, 8709–8712.

[16] a) L. Jaquinod, *The Porphyrin Handbook, Vol. 1*, Academic Press: San Diego, CA, **2000**; b) K. M. Smith, K. C. Langry, O. M. Minnetian, *J. Org. Chem.* **1984**, *49*, 4602–4609; c) W. W. Kalisch, M. O. Senge, *Angew. Chem. Int. Ed.* **1998**, *37*, 1107–1109; d) H. Hata, H. Shinokubo, A. Osuka, *J. Am. Chem. Soc.* **2005**, *127*, 8264–8265.

[17] a) J. Ramesh, S. Sujatha, C. Arunkumar, *RSC Adv.* **2016**, *6*, 63271–63285; b) M. A. Sari, J. P. Battioni, D. Dupre, D. Mansuy, J. B. Le Pecq, *Biochemistry* **1990**, *29*, 4205–4215.

[18] K. Koren, S. M. Borisov, I. Klimant, *Sens. Actuators B* **2012**, *169*, 173–181.

[19] **-. t.** CCDC deposit codes 2213448 (**1-trans**), 2212206 (**1-cis**) contains the supplementary crystallographic data for this paper. These data can be obtained free of charge via www.ccdc.cam.ac.uk/data_request/cif, or by emailing data_request@ccdc.cam.ac.uk, or by contacting The Cambridge Crystallographic Data Centre, 12 Union Road, Cambridge CB2 1EZ, UK; fax: +44 1223 336033.

[20] a) M. O. Senge, T. Ema, K. M. Smith, *J. Chem. Soc. Chem. Commun.* **1995**, 733–734; b) T. Ema, M. O. Senge, N. Y. Nelson, H. Ogoshi, K. M. Smith, *Angew. Chem. Int. Ed.* **1994**, *33*, 1879–1881; c) D. J. Nurco, C. J. Medforth, T. P. Forsyth, M. M. Olmstead, K. M. Smith, *J. Am. Chem. Soc.* **1996**, *118*, 10918–10919.

[21] a) M. W. Renner, J. Fajer, *J. Biol. Inorg. Chem.* **2001**, *6*, 823–830; b) K. M. Kadish, E. Van Caemelbecke, P. Boulas, F. D'Souza, E. Vogel, M. Kisters, C. J. Medforth, K. M. Smith, *Inorg. Chem.* **2002**, *32*, 4177–4178.

[22] a) T. Ogawa, Y. Nishimoto, N. Yoshida, N. Ono, A. Osuka, *Angew. Chem. Int. Ed.* **1999**, *38*, 176–179; b) B. Liu, X. Li, M. Stepien, P. J. Chmielewski, *Chem. Eur. J.* **2015**, *21*, 7790–7797; c) X. Li, Y. Meng, P. Yi, M. Stepien, P. J. Chmielewski, *Angew. Chem. Int. Ed.* **2017**, *56*, 10810–10814.

[23] a) X. Ke, P. Yadav, L. Cong, R. Kumar, M. Sankar, K. M. Kadish, *Inorg. Chem.* **2017**, *56*, 8527–8537; b) N. Chaudhri, L. Cong, A. S. Bulbul, N. Grover, W. R. Osterloh, Y. Fang, M. Sankar, K. M. Kadish, *Inorg. Chem.* **2020**, *59*, 1481–1495.